**Single-stranded regions modulate conformational dynamics and ATPase activity of eIF4A to optimize 5'-UTR unwinding**

Alexandra Zoi Andreou, Ulf Harms & Dagmar Klostermeier

**Supplementary Methods.**

**Electrophoretic mobility shift assays.** Electrophoretic mobility shift assays were performed as described in the main text (Material and Methods) with 100 nM FAM-labeled RNA and equimolar concentrations of the translation initiation factors (as indicated; 1-5% of eIF4A or eIF4B was labeled with Alexa647 to enable fluorescence detection), 4 units of RNAse inhibitor (Roche), 5 mM ATP, 23 µg/ml pyruvate kinase and 1 mM phoshoenolpyruvate in 30 mM Hepes/KOH, pH 7.4, 100 mM KOAc, 3 mM $Mg(OAc)_2$, 2 mM DTT. Complexes were separated by electrophoresis on a 8 % native polyacrylamide gel for 3 h at 170 V. Proteins were detected by Coomassie Brilliant Blue staining, RNA was visualized via FAM fluorescence, eIF4A or eIF4B were detected via Alexa647 fluorescence.

**Supernatant depletion assay.** The interaction eIF4A and eIF4B was tested in supernatant depletion assays performed after Pollard (1). Immobilization of eIF4A on streptavidin beads (Streptavidin Sepharose High Performance, GE Healthcare) was achieved by incubation of 130 µM biotinylated eIF4A in 30 mM Hepes/KOH pH 7.4, 100 mM KOAc, 3 mM $Mg(OAc)_2$, 2 mM DTT for 30 min at room temperature. After centrifugation at 1000 g for 30 s and three washing steps, beads were resuspended in fresh buffer. A total concentration of 0 to 33 µM of eIF4A (immobilized on beads) were mixed with 30 µl of 0.25 µM Alexa488-labeled eIF4B in 30 mM Hepes/KOH pH 7.4, 100 mM KOAc, 3 mM $Mg(OAc)_2$, 2 mM DTT in the presence of 5 µM 20mer RNA, and 10 mM 5´-adenylyl-β,γ-imidotriphosphate, (ADPNP, Sigma Aldrich) for 30 min. After centrifugation at 1000 g, 24 µl of the supernatant were

analyzed by SDS-PAGE. eIF4B was visualized by Alexa488 fluorescence. The fraction bound was determined by densitometry. An experiment with streptavidin beads without eIF4A serves as a negative control.

**Determination of microscopic rate constants from kinetic models.**

*Two distinct closed states*. According to this model (Supplementary Figure 8a), the observed rate constant for closing, $k_{close}$, is

$$k_{close} = k_1 + k_2 \quad \text{(eq. 1)}$$

and the two observed rate constants for closing are

$$k_{open,1} = k_{-1} \quad \text{(eq. 2)}$$

and

$$k_{open,2} = k_{-2} \quad \text{(eq. 3)}$$

The apparent equilibrium constant for closing, $K_{app}$, determined from FRET histograms is

$$K_{app} = \frac{[eIF4A_{closed,1}]+[eIF4A_{closed,2}]}{[eIF4A_{open}]} = K_1 + K_2 \quad \text{(eq. 4)}$$

or

$$K_{app} = \frac{k_1}{k_{-1}} + \frac{k_2}{k_{-2}} \quad \text{(eq. 5)}$$

Combining eq. 1-3 and eq. 5 and solving for $k_1$ gives

$$k_1 = \frac{k_{open,1}\cdot(K_{app}\cdot k_{open,2} - k_{close})}{k_{open,2} - k_{open,1}} \quad \text{(eq. 6).}$$

and

$$k_2 = k_{close} - k_1 \quad \text{(eq. 7).}$$

The rate constants $k_{-1}$ and $k_{-2}$ are identical to the observed rate constants for opening (eq. 2, 3).

*Three distinct closed states.* Inter-conversion of the closed states $eIF4A_{closed,1}$, $eIF4A_{closed,2}$, and $eIF4A_{closed,3}$ with the open state $eIF4A_{open}$ occurs with rate constants $k_1$ and $k_{-1}$, $k_2$ and $k_{-2}$, and $k_3$ and $k_{-3}$ (Supplementary Figure 8b). The observed rate constant for closing, $k_{close}$, is

$$k_{close} = k_1 + k_2 + k_3 \quad \text{(eq. 8)}$$

and the three observed rate constants for closing are

$$k_{open,1} = k_{-1} \quad \text{(eq. 9)}$$

$$k_{open,2} = k_{-2} \quad \text{(eq. 10)}$$

and

$$k_{open,3} = k_{-3} \quad \text{(eq. 11)}$$

The apparent equilibrium constant for closing, $K_{app}$, determined from FRET histograms is

$$K_{app} = \frac{[eIF4A_{closed,1}]+[eIF4A_{closed,2}]+[eIF4A_{closed,3}]}{[eIF4A_{open}]} = K_1 + K_2 + K_3 \quad \text{(eq. 12)}$$

or

$$K_{app} = \frac{k_1}{k_{-1}} + \frac{k_2}{k_{-2}} + \frac{k_3}{k_{-3}} \quad \text{(eq. 13)}$$

This system contains four observables ($k_{close}$, $k_{open,1}$, $k_{open,2}$, $k_{open,3}$, and $K_{app}$) and six unknowns ($k_1$, $k_{-1}$, $k_2$, $k_{-2}$, $k_3$, and $k_{-3}$), and is underdetermined. The appearance of three observed rate constants for opening is not in agreement with the experimental results.

From biochemical analyses it is known that eIF4A can undergo futile cycles (1), in which ATP is hydrolyzed but hydrolysis is not coupled to unwinding, unproductive cycles (2) in which no ATP is hydrolyzed, and the RNA is not unwound, and productive cycles (3), in which ATP hydrolysis is coupled to duplex separation. However, we only observe two conformational cycles of eIF4A in the presence of duplex RNA, indicating that two proceses pass through the same closed state.

*Case 1*. In case 1 (Supplementary Figure 8c), we assume that the ATP-dependent processes 1 and 3 pass through the same closed state, and the inter-conversion with the open state occurs with the same rate constants:

$$k_1 = k_3 \quad \text{(eq. 14)}$$

and

$$k_{-1} = k_{-3} \quad \text{(eq. 15).}$$

The four observables are then related to the microscopic rate constants as

$$k_{close} = k_{13} + k_2 = k_1 + k_3 + k_2 = 2k_1 + k_2 \quad \text{(eq. 16)}$$

$$k_{open,1} = k_{-1} + k_{-3} = 2k_{-1} \quad \text{(eq. 17)}$$

$$k_{open,2} = k_{-2} \quad \text{(eq. 18)}$$

The apparent equilibrium constant for closing, $K_{app}$, determined from FRET histograms is

$$K_{app} = \frac{[eIF4A_{closed,13}]+[eIF4A_{closed,2}]}{[eIF4A_{open}]} = K_{13} + K_2 = \frac{k_1+k_3}{k_{-1}k_{-3}} + \frac{k_2}{k_{-2}} \quad \text{(eq. 19)}$$

From

$$K_{app} = \frac{k_1+k_3}{k_{-1}k_{-3}} + \frac{k_2}{k_{-2}} \quad \text{(eq. 20)}$$

we obtain

$$k_1 = \frac{K_{app} \cdot k_{open,1} \cdot k_{open,2} - k_{close} k_{open,1}}{2(k_{open,2} - k_{open,1})} = k_3 \quad \text{(eq. 21).}$$

The remaining rate constants are then obtained from eq. 16-18 as

$$k_2 = k_{close} - 2k_1 \quad \text{(eq. 22)}$$

$$k_{-1} = \frac{k_{open,1}}{2} = k_{-3} \quad \text{(eq. 23).}$$

and

$$k_{-2} = k_{open,2} \quad \text{(eq. 24)}$$

From the microscopic rate constants determined, the transit times $tt_1$, $tt_2$, and $tt_3$ for futile productive, and unproductive cycles can be calculated.

The transit time $tt_n$ for each cycles is

$$tt_n = \frac{1}{k_n} + \frac{1}{k_{-n}} \quad \text{(eq. 25)}$$

The transit time is related ot the net rate constant for each cycle by

$$k_{net,n} = \frac{1}{tt_n} \quad \text{(eq. 26)}$$

Alternatively, it is conceivable that futile (1) and unproductive cycle (2), both of which do not lead to unwinding, pass through the same closed state. We still assume that the rate constants for the ATP-dependent processes are identical ($k_1$=$k_3$, $k_{-1}$=$k_{-3}$).

In this case (case 2; Supplementary Figure 8d),

$$k_{close} = k_{12} + k_3 = k_1 + k_2 + k_3 = 2k_1 + k_2 \quad \text{(eq. 27)}$$

$$k_{open,1} = k_{-1} + k_{-2} \quad \text{(eq. 28)}$$

$$k_{open,2} = k_{-3} \quad \text{(eq. 29)}$$

The apparent equilibrium constant for closing, $K_{app}$, is

$$K_{app} = \frac{[eIF4A_{closed,12}] + [eIF4A_{closed,3}]}{[eIF4A_{open}]} = K_{12} + K_3 = \frac{k_1 + k_2}{k_{-1}k_{-2}} + \frac{k_3}{k_{-3}} \quad \text{(eq. 30)}$$

which gives

$$k_1 = \frac{K_{app} \cdot k_{open,1} \cdot k_{open,2} - k_{close} k_{open,2}}{(k_{open,1} - k_{open,2})} = k_3 \quad \text{(eq. 31).}$$

The remaining rate constants are then obtained from eq. 27-29 as

$$k_2 = k_{close} - 2k_1 \quad \text{(eq. 32).}$$

$$k_{-1} = k_{open,2} = k_{-3} \quad \text{(eq. 33).}$$

and

$$k_{-2} = k_{open,1} - k_{open,2} \quad \text{(eq. 34).}$$

This model leads to negative values for $k_2$ and $k_{-2}$, and can thus be discarded.

**Supplementary Figures**

Supplementary Figure 1: **Effect of the concentration of eIF4B on eIF4A dynamics.**

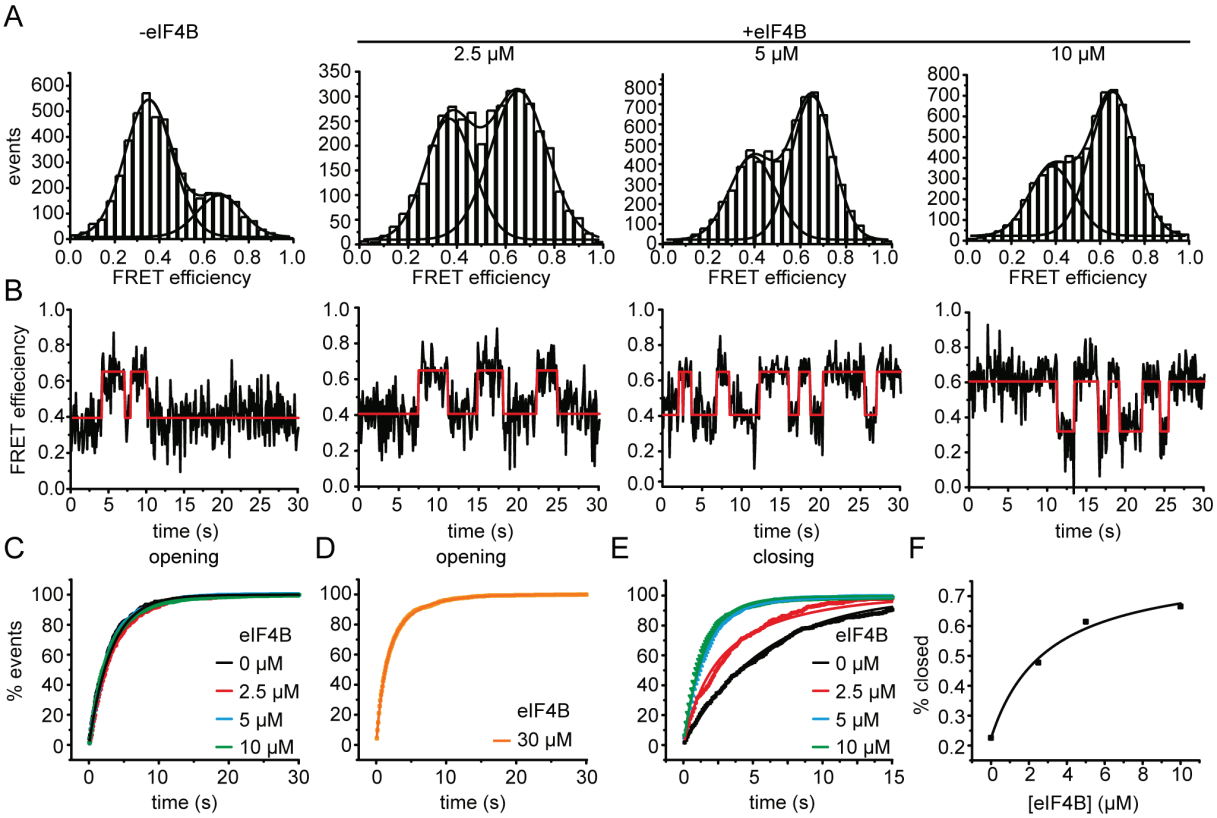


**A**: FRET histograms for eIF4A in the presence of 10 μM eIF4G, 3 mM ATP, and 15 μM 50mer RNA with increasing concentrations of eIF4B (0, 2.5, 5, and 10 μM).

**B**: Representative FRET time traces from the experiments shown in A.

**C**: Normalized CDHs for opening of eIF4A and global fit using single-exponential functions. The rate constant of opening, $k_{open}$ = 0.31 $s^{-1}$, is independent of eIF4B.

**D**: Double-exponential fit to the normalized CDH for opening of eIF4A in the presence of 30 μM eIF4B.

**E**: CDHs for closing for experiments shown in A, and global fit with double-exponential functions. eIF4A closes with $k_{close,1}$ = 0.17 $s^{-1}$ (closing of eIF4A/G) and $k_{close,2}$ = 0.69 $s^{-1}$ (closing of eIF4/B/G).

**F**: Percentage of eIF4A in the closed state as a function of the concentration of eIF4B.

Supplementary Figure 2: **Single-exponential fits of normalized CDHs for opening and closing of eIF4A in presence of ssRNAs.**

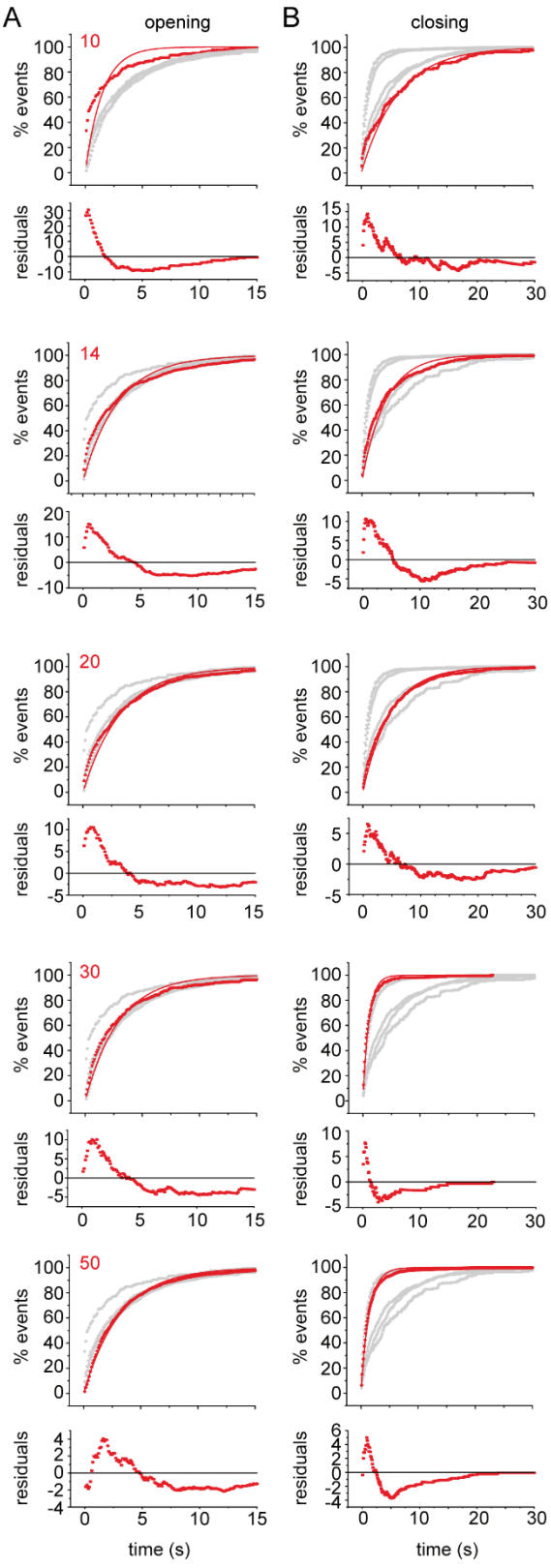


Figure legend on next page.

**A**: Normalized CDH for opening, single-exponential fits, and residuals.

**B**: Normalized CDH for closing, single-exponential fits, and residuals.

The respective histogram and the fit are shown in red, the histograms for all RNAs are depicted in gray. See Supplementary Table 1 for the associated $R^2$-values. 10, 14, 20, 30, 50: 10mer, 14mer, 20mer, 30mer, 50mer.

Supplementary Figure 3: **Double-exponential fits of normalized CDHs for opening and closing of eIF4A in presence of ssRNAs.**

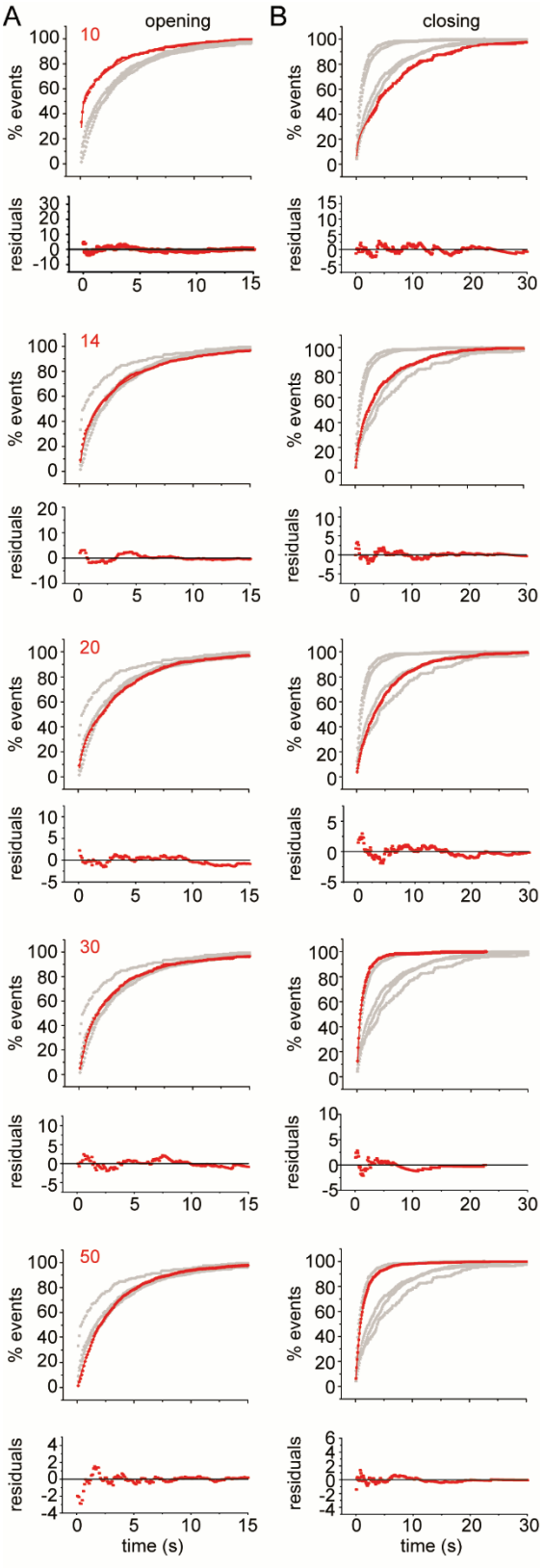


Figure legend on next page.

**A**: Normalized CDHs for opening, double-exponential fits, and residuals.

**B**: Normalized CDHs for closing, double-exponential fits, and residuals.

The respective histogram and the fit are highlighted in red, the histograms for all RNAs are depicted in gray for comparison. See Supplementary Table 1 for the associated $R^2$-values. 10, 14, 20, 30, 50: 10mer, 14mer, 20mer, 30mer, 50mer.

Supplementary Figure 4: **Binding of eIF4B to eIF4A in the presence of the 20mer.**

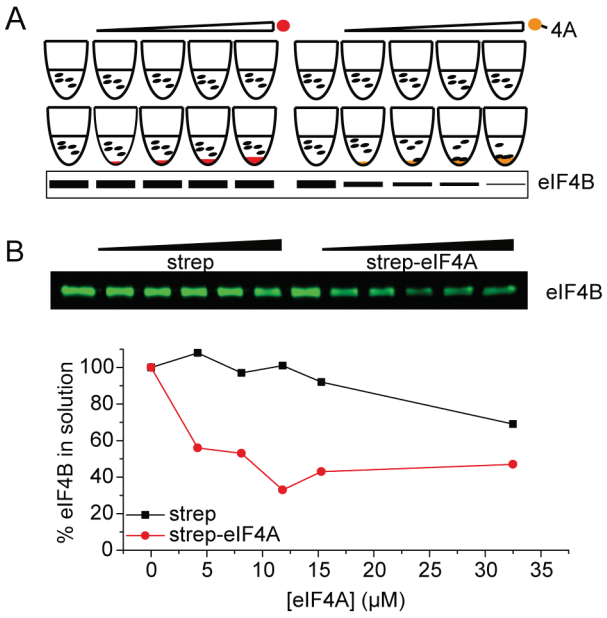


**A**: Principle of the supernatant depletion assay (reprinted from Andreou A.Z., Harms U., Klostermeier D. (2017) RNA Biol. 14(1):113-123, with permission) (1). Biotinylated eIF4A is immobilized on streptavidin-coated beads (orange), a constant concentration of 0.25 µM eIF4B is in the supernatant. A control experiment is performed with streptavidin-functionalized beads without eIF4A (red).

**B**: Supernatant depletion assay. PAGE analysis of Alexa488-labeled eIF4B in the supernatant (top) and quantification (bottom).

Supplementary Figure 5: **Single-exponential fits of CDHs for opening and closing in the presence of dsRNAs.**

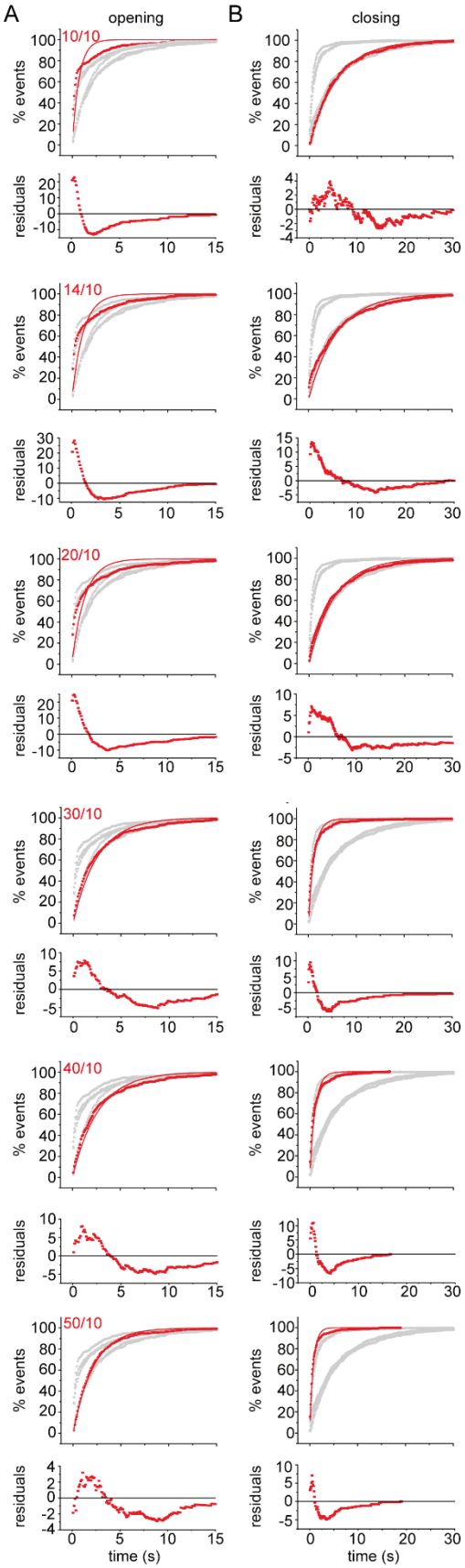


Figure legend on next page.

**A**: Normalized CDHs for opening, single-exponential fits, and residuals.

**B**: Normalized CDHs for closing, single-exponential fits, and residuals.

The respective histogram and the fit are highlighted in red, the histograms for all RNAs are depicted in gray for comparison. See Supplementary Table 1 for the associated $R^2$-values. 10/10, 14/10, 20/10, 30/10, 40/10, 50/10: 10/10mer, 14/10mer, 20/10mer, 30/10mer, 40/10mer, 50/10mer.

Supplementary Figure 6: **Double-exponential fits of CDHs for opening and closing in the presence of dsRNAs.**

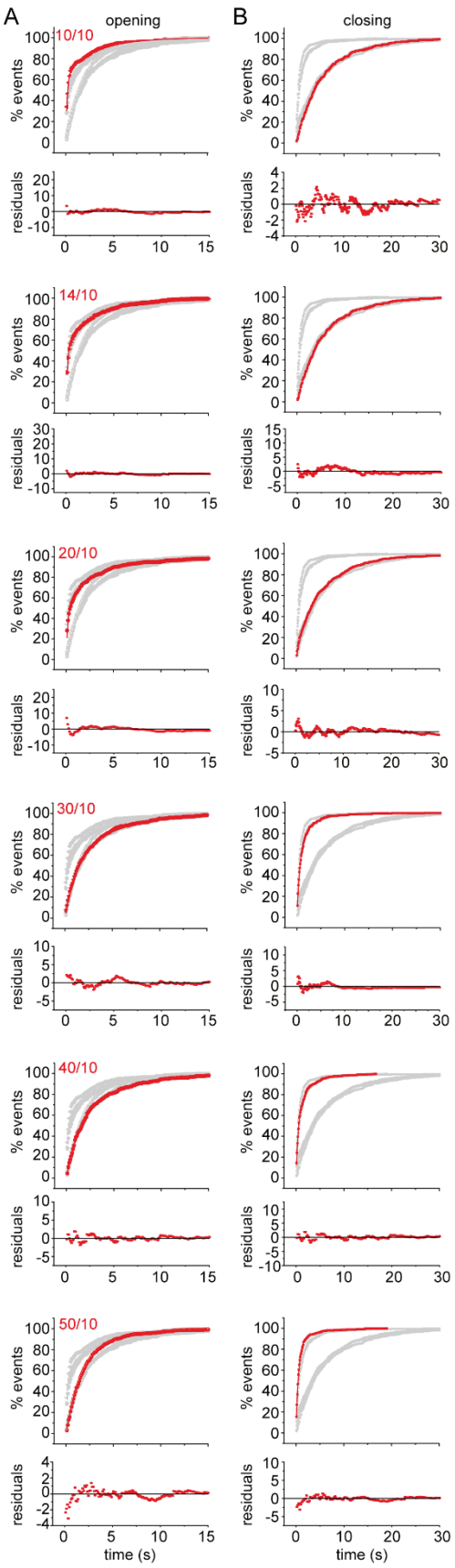


Figure legend on next page.

**A**: Normalized CDHs for opening, double-exponential fits, and residuals.

**B**: Normalized CDHs for closing, double-exponential fits, and residuals. The respective histogram and the fit are highlighted in red, the histograms for all RNAs are depicted in gray for comparison. See Supplementary Table 1 for the associated $R^2$-values. 10/10, 14/10, 20/10, 30/10, 40/10, 50/10: 10/10mer, 14/10mer, 20/10mer, 30/10mer, 40/10mer, 50/10mer.

Supplementary Figure 7: **Anisotropy titrations of the 20/10mer and 30/10mer RNAs with eIF4B, eIF4A/G, and eIF4G.**

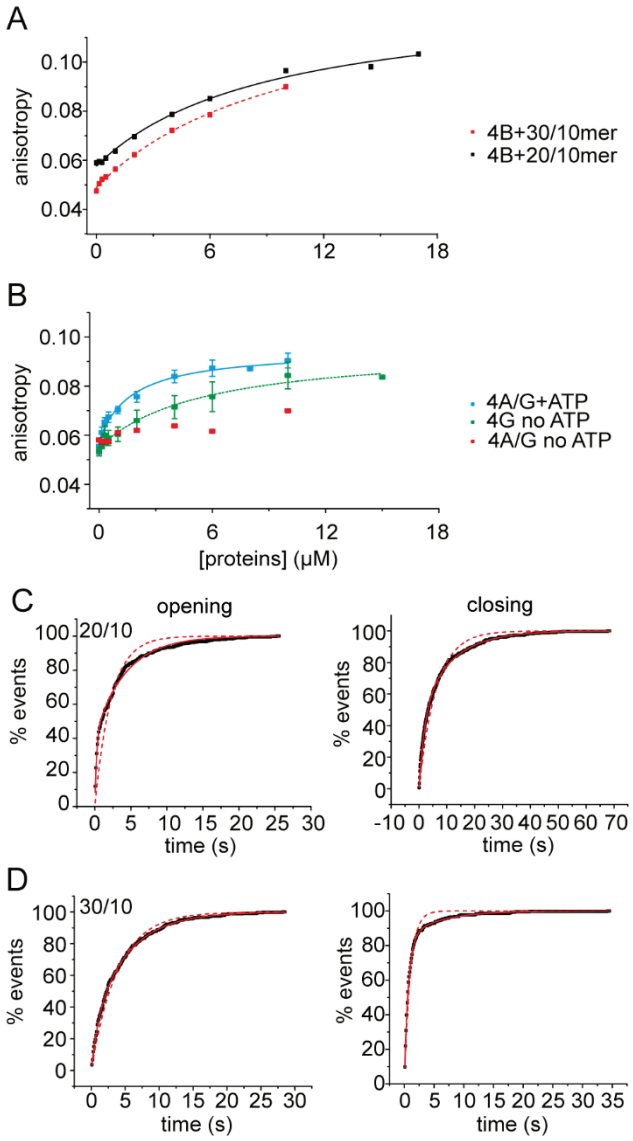


**A**: Fluorescence anisotropy titrations of 0.05 μM of the 20/10mer and 30/10mer RNAs with eIF4B.

**B:** Titrations of 0.05 μM of 30/10mer RNA with eIF4G or eIF4A/G in the absence and presence of 5 mM ATP. The $K_d$ values are 3.8 (±1.2) μM (eIF4G), n.d. (eIF4A/G, no ATP), and 1.6 (±0.5) μM (eIF4A/G, ATP).

**C**: Normalized CDHs for opening and closing of eIF4A in the presence of 45 μM 20/10mer RNA. Single-exponential fits are depicted as dashed lines, double-exponential fist as solid lines. The rate constants are $k_{open,1}$ = 0.24 $s^{-1}$ (59% amplitude) and $k_{open,2}$ = 4.3 $s^{-1}$ (41% amplitude), and $k_{close}$ = 0.18 $s^{-1}$.

**D**: Normalized CDHs for opening and closing of eIF4A in the presence of 45 µM 30/10mer RNA. Single-exponential fits are depicted as dashed lines, double-exponential fit as a solid lines. The rate constants are $k_{open,1}$ = 0.19 $s^{-1}$ (73% amplitude) and $k_{open,2}$ = 0.99 $s^{-1}$ (27% amplitude), and $k_{close,1}$ = 0.18 $s^{-1}$ (84% amplitude) and $k_{close,2}$ = 1.5 $s^{-1}$ (16% amplitude). 20/10: 20/10mer, 30/10: 30/10mer.

Supplementary Figure 8: **Binding of RNA to eIF4A and its complexes.**

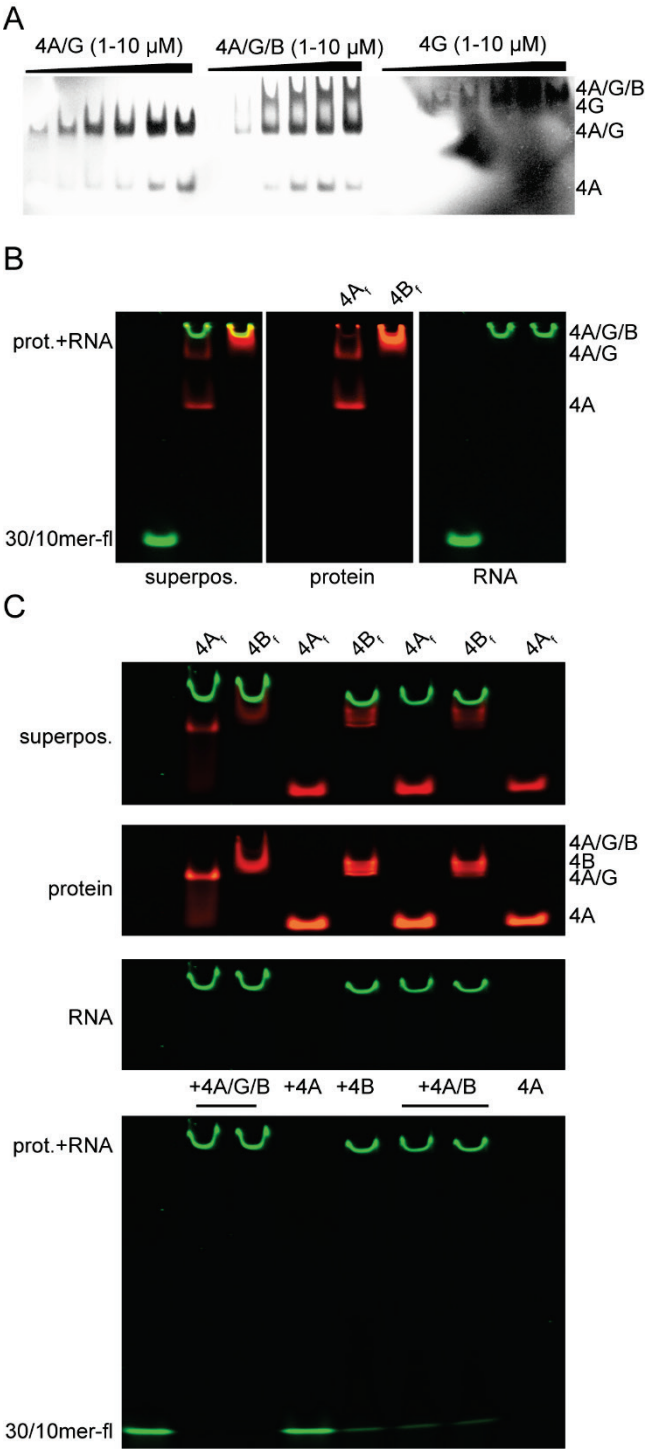


**A**: Electrophoretic mobility shift assay of 100 nM fluorescein-labeled RNA (see Figure 6) with increasing concentrations of eIF4G, eIF4A and eIF4G, or eIF4A, eIF4B, and eIF4G, after Coomassie-blue staining. The last lane in each series does not contain RNA. eIF4G has a low electrophoretic mobility. With eIF4A and eIF4G, two species are detected. The species with the higher electrophoretic mobility corresponds to eIF4A, the species with the lower electrophoretic mobility is eIF4A/G, which migrates faster than

eIF4G alone. When eIF4B is also present, a third band with even lower mobility is detected, which represents the A/B/G complex (see panel B).

**B**: Electrophoretic mobility shift assay of 100 nM fluorescein-labeled 30/10mer RNA (green) with 10 µM eIF4A, eIF4B, and eIF4G. $4A_f$: 100 nM Alexa647-labeled eIF4A; $4B_f$: 100 nM Alexa647-labeled eIF4B (red). The first lane shows the RNA-only control. In the presence of eIF4A, eIF4B, and eIF4G, the RNA shows a reduced electrophoretic mobility, consistent with binding to the translation initiation factors. With $4A_f$, three species are detected: free eIF4A (lowest electrophoretic mobility), eIF4A/G (intermediate electrophoretic mobility) and eIF4A/B/G (highest electrophoretic mobility, bound to RNA). The band for the eIF4A/B/G complex is faint as the concentration of the complex is limited by the concentration of RNA present (100 nM). With $4B_f$, a broad band is detected that corresponds to free eIF4B and the eIF4A/B/G complex that is bound to and comigrates with the RNA.

**C**: Electrophoretic mobility shift assay of 100 nM fluorescein-labeled 30/10mer RNA (green) with 10 µM eIF4A, eIF4B, and eIF4G, 10 µM eIF4A, 10 µM eIF4B, 10 µM eIF4A and eIF4B, and 10 µM eIF4A in the absence of RNA. The first lane shows the RNA-only control. $4A_f$: 100 nM Alexa647-labeled eIF4A; $4B_f$: 100 nM Alexa647-labeled eIF4B (red). The RNA shows an electrophoretic mobility shift with eIF4B, with eIF4A and eIF4B, and with eIF4A, eIF4B, and eIF4G, consistent with protein binding. The electrophoretic mobility of the RNA in the presence of all three factors is lower than in the presence of eIF4A and eIF4B, indicating that it represents RNA bound to the eIF4A/B/G complex.

Supplementary Figure 9: **Kinetic models and biochemical interpretation.**

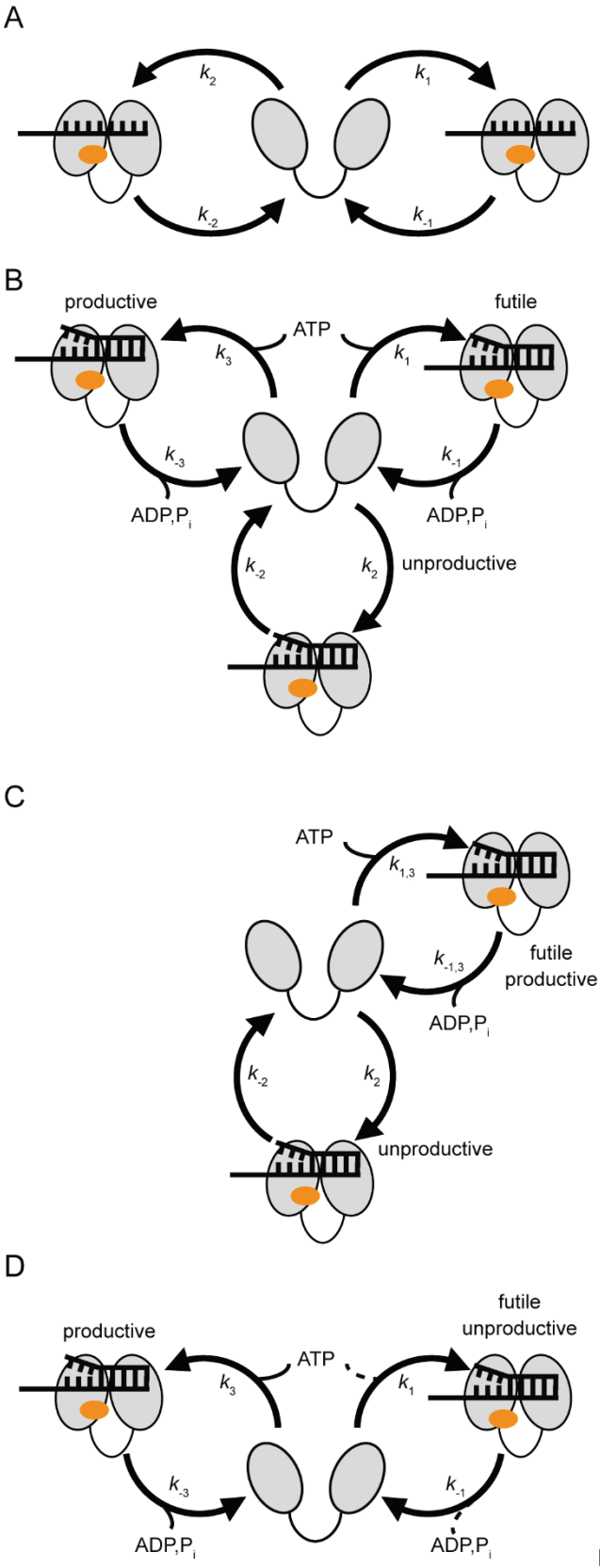


Figure legend on next page.

**A**: Model with one open and two kinetically and functionally distinct closed states of eIF4A, linked by two alternative conformational cycles.

**B**: Model with one open and three kinetically and functionally distinct closed states of eIF4A. The individual cycles could reflect futile cycles (1: ATP hydrolysis, but no unwinding,), unproductive cycles (2: no unwinding, no ATP hydrolyzed), and productive cycles (3: unwinding and ATP hydrolysis).

**C**: Model with one open and two kinetically and functionally distinct closed states of eIF4A, with futile and productive cycles (1, 2) passing through the same closed state. If these ATP-dependent processes occur with the same rate constants, all six microscopic rate constants can be determined (see Supplementary Methods; Case 1).

**D**: Model with one open and two kinetically and functionally distinct closed states of eIF4A, with futile and unproductive cycles (1, 2) passing through the same closed state. The six rate microscopic rate constants can be determined under the assumption that opening and closing in ATP-dependent (futile and productive) cycles occur with the same rate constants (see Supplementary Methods; Case 2).

**Supplementary Tables**

**Supplementary Table 1:** $R^2$-values for single- and double-exponential fits of CDHs for eIF4A opening and closing

| | opening | | | closing | | |
|---|---|---|---|---|---|---|
| RNA | sexp | dexp | factor | sexp | dexp | factor |
| 10mer | 0.757 | 0.992 | 1.309 | 0.983 | 0.998 | 1.015 |
| 14mer | 0.959 | 0.998 | 1.041 | 0.973 | 0.999 | 1.027 |
| 20mer | 0.982 | 0.999 | 1.017 | 0.995 | 0.999 | 1.004 |
| 30mer | 0.981 | 0.998 | 1.017 | 0.986 | 0.997 | 1.011 |
| 50mer | 0.997 | 0.999 | 1.002 | 0.990 | 0.999 | 1.010 |
| 10/10mer | 0.707 | 0.993 | 1.404 | 0.998 | 0.999 | 1.001 |
| 14/10mer | 0.742 | 0.998 | 1.346 | 0.978 | 0.998 | 1.021 |
| 20/10mer | 0.813 | 0.992 | 1.220 | 0.991 | 0.999 | 1.008 |
| 30/10mer | 0.982 | 0.999 | 1.017 | 0.968 | 0.997 | 1.030 |
| 40/10mer | 0.984 | 0.999 | 1.015 | 0.958 | 0.998 | 1.041 |
| 50/10mer | 0.996 | 0.999 | 1.003 | 0.977 | 0.999 | 1.022 |

Fits and residuals are shown in Supplementary Figures 2 and 3 (single-stranded RNAs), and Supplementary Figures 5 and 6 (double-stranded RNAs). sexp: single-exponential fit; dexp: double-exponential fit; factor: fold decrease in $R^2$ for double-exponential fit.

**Supplementary Table 2:** Bayesian information criterion (BIC) from the analysis of single-molecule data with the program SMACKS (2).

| | ΔBIC | |
|---|---|---|
| RNA | oc | occ |
| 20mer | 0 | 53 |
| 14/10mer | 0 | -602 |
| 20/10mer | 0 | -669 |
| 30/10mer | 0 | -11 |
| 50/10mer | 0 | 101 |

oc: model with one open and one closed state, occ: model with one open and two (non-interconverting) closed states. A ΔBIC below -5 indicates a higher probability for the occ model to be consistent with the data.

**Supplementary Table 3a:** Microscopic rate constants for a model with two alternative conformational cycles, with one cycle reflecting ATP-dependent processes (futile and productive cycles), and the second reflecting unproductive cycles (case 1; see Supplementary Methods).

| | closing | | | opening | | |
|---|---|---|---|---|---|---|
| RNA | $k_1$ ($s^{-1}$) | $k_2$ ($s^{-1}$) | $k_3$ ($s^{-1}$) | $k_{-1}$ ($s^{-1}$) | $k_{-2}$ ($s^{-1}$) | $k_{-3}$ ($s^{-1}$) |
| 10/10mer | 0.012 | 0.146 | 0.012 | 0.15 | 5.8 | 0.15 |
| 14/10mer | 0.015 | 0.139 | 0.015 | 0.145 | 6.1 | 0.145 |
| 20/10mer | 0.025 | 0.141 | 0.025 | 0.13 | 4.4 | 0.13 |
| 30/10mer | 0.109 | 0.602 | 0.109 | 0.105 | 0.86 | 0.105 |
| 40/10mer | 0.193 | 0.524 | 0.193 | 0.095 | 0.72 | 0.095 |
| 50/10mer | 0.174 | 0.953 | 0.174 | 0.1 | 0.59 | 0.1 |

1: futile cycles, 2: unproductive cycles, 3: productive cycles

**Supplementary Table 3b:** Transit times *tt*, net rate constants $k_{net}$, and *flux* through each conformational cycle (case 1; see Supplementary Methods).

| | $tt_{13}$ (s) | $tt_2$ (s) | $k_{13net}$ ($s^{-1}$) | $k_{2net}$ ($s^{-1}$) | $flux_{13}$ | $flux_2$ |
|---|---|---|---|---|---|---|
| 10/10mer | 44.3 | 7.0 | 0.023 | 0.142 | 0.137 | 0.863 |
| 14/10mer | 36.2 | 7.3 | 0.028 | 0.136 | 0.168 | 0.832 |
| 20/10mer | 24.2 | 7.3 | 0.041 | 0.136 | 0.232 | 0.768 |
| 30/10mer | 9.3 | 2.8 | 0.107 | 0.354 | 0.232 | 0.768 |
| 40/10mer | 7.9 | 3.3 | 0.127 | 0.303 | 0.295 | 0.705 |
| 50/10mer | 7.9 | 2.7 | 0.126 | 0.364 | 0.258 | 0.742 |

1: futile cycles, 2: unproductive cycles, 3: productive cycles

**Supplementary References**


1. Pollard, T.D. (2010) A guide to simple and informative binding assays. *Mol. Biol. Cell*, **21**, 4061-4067.
2. Schmid, S., Gotz, M. and Hugel, T. (2016) Single-Molecule Analysis beyond Dwell Times: Demonstration and Assessment in and out of Equilibrium. *Biophys. J.*, **111**, 1375-1384.